Scientific Research Publishing

Open Journal of Internal Medicine, 2026, 16(2), 313-331
https://www.scirp.org/journal/ojim
ISSN Online: 2162-5980
ISSN Print: 2162-5972

Based on Bioinformatics Analysis of Ferroptosis-Immune Interaction Core Genes and Immune Infiltration Characteristics in Alzheimer's Disease

Junwei Ma[1,2], Yuxuan Li[3], Ruijie Zheng[3], Chongdong Jian[1*]

[1]Department of Neurology, Affiliated Hospital of Youjiang Medical University for Nationalities, Baise, China
[2]Graduate School, Youjiang Medical University for Nationalities, Baise, China
[3]Youjiang Medical University for Nationalities, Baise, China
Email: *1944045826@qq.com

How to cite this paper: Ma, J.W., Li, Y.X., Zheng, R.J. and Jian, C.D. (2026) Based on Bioinformatics Analysis of Ferroptosis-Immune Interaction Core Genes and Immune Infiltration Characteristics in Alzheimer's Disease. *Open Journal of Internal Medicine*, **16**, 313-331.
https://doi.org/10.4236/ojim.2026.162024

Received: May 3, 2026
Accepted: June 6, 2026
Published: June 9, 2026

Abstract

Objective: This study aims to systematically screen the core genes co-regulated by ferroptosis and immunity in Alzheimer's disease (AD) through bioinformatics analysis, construct a multi-level molecular network, provide a theoretical basis for revealing the molecular mechanism of the interaction between ferroptosis and the immune microenvironment in AD, enrich the pathological connotation of neuroinflammation and iron metabolism disorders, and offer potential intervention targets and new research ideas for the diagnosis and immune-targeted therapy of AD. **Methods:** The GSE5281 dataset was downloaded from the Gene Expression Omnibus (GEO) as the analysis object. The limma package in the R language was used to screen differentially expressed genes (DEGs). Intersection genes between ferroptosis-related and immunity-related DEGs were obtained by cross-referencing with the FerrDb and ImmPort databases. Subsequently, GO and KEGG enrichment analyses were performed to elucidate the functions and pathways of the candidate genes. To visualize protein-protein interactions, STRING, Cytoscape, and Cytohubba were used to construct a protein-protein interaction network and screen core hub genes. The CIBERSORT algorithm was employed to estimate the infiltration abundance of 22 immune cell types, generate stacked bar plots, and compare immune infiltration levels between the AD and control groups using the Wilcoxon test with FDR multiple-testing correction; intergroup differences were displayed via boxplots. **Results:** Intersecting the 1191 DEGs from the GSE5281 dataset with ferroptosis and immunity gene sets yielded 54 ferroptosis-immunity intersection DEGs. Functional enrichment analysis showed that these genes were predominantly involved in negative regulation of immune system processes, monocyte differentiation, lymphocyte pro-

liferation, and vesicle lumen components, and were significantly enriched in the TNF signaling pathway, lipid metabolism-related pathways, and immune inflammation-related pathways. Topological analysis of the PPI network using Cytoscape and the MCC algorithm in CytoHubba identified five core hub genes: BCL2, CD44, FOXO1, PPARG, and SOX2. Immune infiltration stacked bar plots showed marked differences in immune cell composition between the AD and control groups, with the AD group exhibiting an overall shift toward a pro-inflammatory, activated immune state. After FDR correction, boxplots further demonstrated that, compared with the control group, the AD group had significantly elevated infiltration proportions of memory B cells, $CD8^+$ cytotoxic T cells, eosinophils, and neutrophils ($P < 0.05$, $P < 0.001$), and significantly reduced proportions of follicular helper T cells, resting NK cells, M0 macrophages, M1 macrophages, and M2 macrophages ($P < 0.05$, $P < 0.01$, $P < 0.001$). These results indicate that the AD brain immune microenvironment undergoes remodeling characterized by the coexistence of pro-inflammatory activation and homeostatic imbalance. **Conclusion:** This study screened and identified five core hub genes for ferroptosis-immune interaction in AD: BCL2, CD44, FOXO1, PPARG, and SOX2. Functional enrichment revealed their significant involvement in immune inflammation-related pathways such as the TNF signaling pathway and lipid metabolism. Immune infiltration analysis found that AD brain tissue exhibits microenvironment remodeling characterized by increased infiltration of pro-inflammatory immune cells and decreased resting innate immune cells. These findings provide new molecular target combinations and a theoretical basis for the early diagnosis of AD and combined immune-ferroptosis targeted therapy.

Keywords

Alzheimer's Disease, Ferroptosis, Immune Microenvironment, Bioinformatics, Immune Infiltration

1. Introduction

Alzheimer's disease (AD) is the leading cause of dementia worldwide. With the aging population, its incidence continues to rise, posing a serious public health issue. Among approximately 55 million dementia patients globally, 60% - 80% have AD, and the number of affected individuals is projected to exceed 150 million by 2050. This disease leads to the loss of self-care ability in patients, imposing a heavy burden on families and society. Currently, clinical diagnosis of AD mainly relies on clinical symptoms, imaging, and cerebrospinal fluid biomarkers, lacking effective early diagnostic methods. In terms of treatment, only a few drugs can briefly delay the disease progression, but none can reverse or halt the disease [1]. Therefore, in-depth exploration of the pathological mechanisms of AD and the search for early diagnostic markers and new therapeutic targets are of urgent clinical need and significant scientific value.

In recent years, ferroptosis, an iron-dependent, lipid peroxidation-driven form

of programmed cell death, has garnered widespread attention in neurodegenerative diseases. Its typical features include intracellular iron accumulation, reduced GPX4 activity, and excessive accumulation of lipid reactive oxygen species (ROS) [2]. Studies have shown iron metabolism disorders in the brain tissue of AD patients, such as elevated ferritin, altered transferrin receptor expression, and abnormal iron deposition, which are significantly correlated with cognitive decline [3]. Meanwhile, immune microenvironment dysregulation, particularly persistent microglial activation and neuroinflammation, is also a hallmark of AD pathology [4]. Research has revealed a bidirectional regulation between ferroptosis and immune responses: DAMPs released by ferroptosis can activate the NLRP3 inflammasome, exacerbating neuroinflammation [5]; while activated microglia and T lymphocytes disrupt brain iron homeostasis by secreting inflammatory factors, promoting ferroptosis [6]. Currently, there is ample evidence on the individual roles of ferroptosis or immune mechanisms in AD, but the molecular mechanisms of their synergistic regulation remain systematically unclear.

To fill this gap, this study starts from the perspective of the interaction between ferroptosis and the immune microenvironment, aiming to elucidate the molecular basis of their synergistic dysregulation in AD. Existing studies are mostly limited to single-omics analysis, failing to simultaneously incorporate ferroptosis and immune genes, and lacking deep integration of gene expression with immune cell infiltration, which restricts a holistic understanding of the "iron metabolism-immune inflammation" axis in AD [7]. Therefore, this study proposes and implements for the first time a bioinformatics strategy integrating cross-analysis of ferroptosis and immune genes, protein-protein interaction network construction, and comprehensive immune infiltration assessment to address the shortcomings of current research.

Based on the GSE5281 transcriptome dataset, this study integrates ferroptosis- and immune-related gene sets from the FerrDb and ImmPort databases for multi-level analyses: screening and cross-analysis of differentially expressed genes (DEGs) to identify co-regulated genes in AD; GO and KEGG enrichment analysis to reveal key biological processes and pathways; PPI network construction using STRING and Cytoscape to screen hub genes; and estimation of the infiltration abundance of 22 immune cell types using CIBERSORT. This integrated strategy combines the advantages of high-throughput data mining and systematic analysis. The main objectives include: screening core genes and elucidating their biological functions and involved inflammatory pathways; quantifying immune infiltration characteristics to construct an integrated analysis framework from molecular features to cellular phenotypes. The results of this study are expected to expand the "immune-iron metabolism" hypothesis of AD and provide potential intervention targets for targeted therapy.

2. Materials and Methods

2.1. Data Sources

We downloaded the GSE5281 dataset from the Gene Expression Omnibus (GEO)

as the analysis object. This dataset, based on the GPL570 platform, includes gene expression profiles of brain tissue samples from 87 AD patients and 73 healthy controls, with sample regions covering AD-related brain areas such as the hippocampus and temporal cortex. The ferroptosis-related gene list was downloaded from the FerrDb database (http://www.zhounan.org/ferrdb/), and the immune-related gene list was downloaded from the ImmPort database (https://www.immport.org/).

The relevant gene sets were integrated from the following sources: 1) The FerrDb database (version V2.0, downloaded on April 20, 2026), yielding a total of 621 protein-coding ferroptosis-related genes (including 264 drivers, 238 suppressors, 9 markers, and 110 unclassified genes); 2) Ferroptosis-related non-coding RNAs were integrated from miRBase (v22.1), CircBank (v3.0), and LncBase (v2.0); 3) Supplementary literature-reported ferroptosis-associated genes (e.g., RPL8, MIOX) were added. A final ferroptosis-related gene set comprising protein-coding genes, miRNAs, circRNAs, and lncRNAs was compiled for subsequent intersection analysis. The immune-related gene list was downloaded from the ImmPort database (Release 61, downloaded on April 20, 2026), yielding a total of 3,118 immune-related genes. This gene set was obtained by integrating core genes from 17 immune-related pathways in ImmPort and supplementing with literature-reported immune regulatory genes to ensure coverage of key nodes in AD-related immune-inflammatory regulation.

2.2. Data Preprocessing

Preprocessing of the GSE5281 dataset was performed using R software (version 4.3.1), with the following specific steps:

Data Reading: The raw expression matrix of the dataset was read using the affy and GEOquery packages in R, extracting sample information and gene expression data.

Background Correction: The robust multi-array average (RMA) algorithm was used for background correction of raw data to eliminate background noise interference during chip hybridization.

Quantile Normalization: The corrected expression matrix was quantile-normalized using the limma package to ensure consistent gene expression distribution across all samples in both datasets, eliminating systematic errors between samples and ensuring comparability.

Probe Annotation: Chip probe IDs were converted to corresponding gene symbols, and probes that could not be matched to gene names were removed. Additionally, low-expression genes in the lowest 25% across all samples were removed to avoid interference in subsequent analyses.

Sample Cleaning: Principal component analysis (PCA) was performed to identify outliers. After PCA analysis, four outlier samples were identified and removed (including sample GSM119676), and a final set of 83 AD samples and 69 control samples (totaling 152 samples) was retained for subsequent analysis.

2.3. Screening of Differentially Expressed Genes

We used the "limma" package to screen for differentially expressed genes (DEGs)

in the dataset, with thresholds set at adjusted $p < 0.05$ and $|\log_2 \text{fold change (FC)}| \geq 1$. The analytical model included disease status (AD vs. control) as the main effect, without incorporating brain region as a covariate. After obtaining significantly differentially expressed genes, we used the "pheatmap" and "ggplot2" R packages to create volcano plots to visualize the distribution of DEGs.

2.4. Identification of Ferroptosis-Immune Intersection Differentially Expressed Genes

The ferroptosis-related gene list from FerrDb and the immunity-related gene list from ImmPort were intersected with the DEGs to obtain ferroptosis- and immunity-related intersection DEGs, designated as Immunity- and Ferroptosis-Related Differentially Expressed Genes (IF-DEGs), which served as the candidate gene set for subsequent analyses.

2.5. Functional Enrichment Analysis

We used the "clusterProfiler" R package for Gene Ontology (GO) and Kyoto Encyclopedia of Genes and Genomes (KEGG) pathway enrichment analysis of the candidate genes. GO analysis covered three categories: biological process (BP), cellular component (CC), and molecular function (MF). Adjusted $P < 0.05$ was used as the significance threshold to filter statistically significant enrichment terms and signaling pathways.

2.6. Protein-Protein Interaction Network Construction and Core Gene Screening

We used the Search Tool for the Retrieval of Interacting Genes/Proteins (STRING) database to construct a PPI network of IM-DEGs, with a confidence threshold set at ≥0.700 (high confidence), and unconnected isolated nodes were hidden. Subsequently, we used Cytoscape 3.10.1 software for network visualization. Furthermore, using the CytoHubba plugin in Cytoscape, we employed the Maximal Clique Centrality (MCC) algorithm to identify the top 5 core hub genes.

2.7. Gene Set Enrichment Analysis

We performed Gene Set Enrichment Analysis (GSEA) based on the whole-genome expression profile, using KEGG and Reactome gene sets as references. Based on the normalized enrichment score (NES) and adjusted P value, we identified signaling pathways significantly activated or suppressed in the AD group, verifying the regulatory characteristics of immune-related pathways in AD at a global level.

2.8. Immune Infiltration Analysis

We used the CIBERSORT algorithm to estimate the relative infiltration abundance of 22 immune cell types in each sample, and drew stacked bar plots of immune cells to visually display differences in immune cell composition between samples.

Intergroup comparisons of immune cell infiltration levels were conducted using the Wilcoxon rank-sum test, followed by false discovery rate (FDR) multiple-testing correction, with differences displayed via boxplots. An FDR-adjusted $P < 0.05$ was considered statistically significant.

2.9. Statistical Analysis

All data analyses were performed in the R software environment (version 4.3.1). Measurement data were expressed as mean ± standard deviation. Comparisons between groups were performed using t-tests or Wilcoxon rank-sum tests, depending on data distribution. The significance criteria for differential gene screening were $|\log_2 FC| \geq 1$ and adjusted $P < 0.05$; the significance criterion for enrichment analysis was adjusted $P < 0.05$. All tests were two-sided, and $P < 0.05$ was considered statistically significant.

3. Results

3.1. Identification of Differentially Expressed Genes

After RMA background correction, quantile normalization, and PCA-based removal of four outlier samples, 83 AD samples and 69 control samples were ultimately included, and the quality of the analyzed samples was good. Principal component analysis results showed that the AD group samples were concentrated with high intra-group homogeneity; outlier samples in the control group had been removed, and there was a clear transcriptomic separation trend between the two groups, suggesting systematic differences in gene expression profiles of brain tissue between AD and healthy controls (**Figure 1(a)**).

Using adjusted $P < 0.05$ and $|\log_2 FC| \geq 1$ as screening thresholds, a total of 1191 DEGs were identified between the AD group and the control group. The number of differentially expressed genes under this threshold ensured both the biological significance of expression changes and avoided the loss of valid genes due to overly strict thresholds. The volcano plot clearly displayed the distribution of expression fold changes and statistical significance for all genes: red dots represent significantly upregulated genes, blue dots represent significantly downregulated genes, and gray dots represent genes without statistical differences, with slightly more upregulated genes than downregulated ones, indicating widespread disease-specific transcriptomic disruption in AD brain tissue (**Figure 1(b)**).

3.2. Identification of Intersection Genes between Ferroptosis-Related and Immunity-Related DEGs

To focus on key genes intersecting ferroptosis and immune regulation in AD, the above DEGs were intersected with ferroptosis-related genes from the FerrDb database and immune-related genes from the ImmPort database. Venn diagram results showed that a total of 54 co-associated differentially expressed genes belonging to all three gene sets were obtained (Immunity- and Ferroptosis-Related Dif-

ferentially Expressed Genes, IF-DEGs) (Figure 2). These genes were defined as candidate gene sets for subsequent analysis to explore the cross-mechanism of ferroptosis and immune regulation in AD.

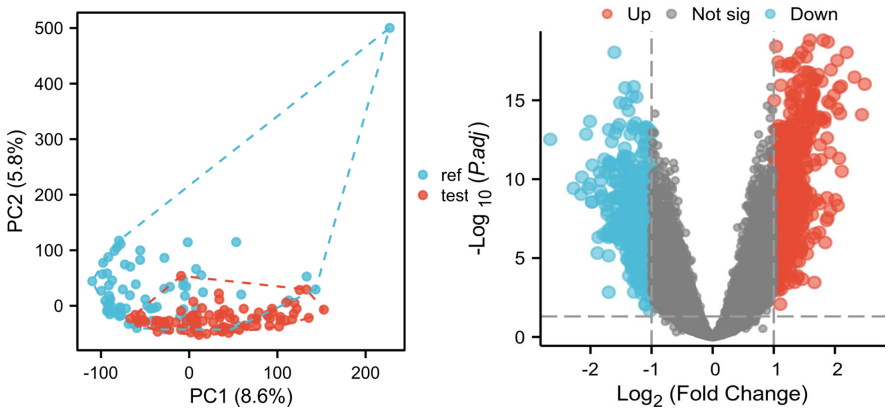

(a) (b)

Figure 1. Identification of differentially expressed genes. (a) Principal component analysis of the expression microarray dataset from AD patients; (b) Volcano plot of differentially expressed genes.

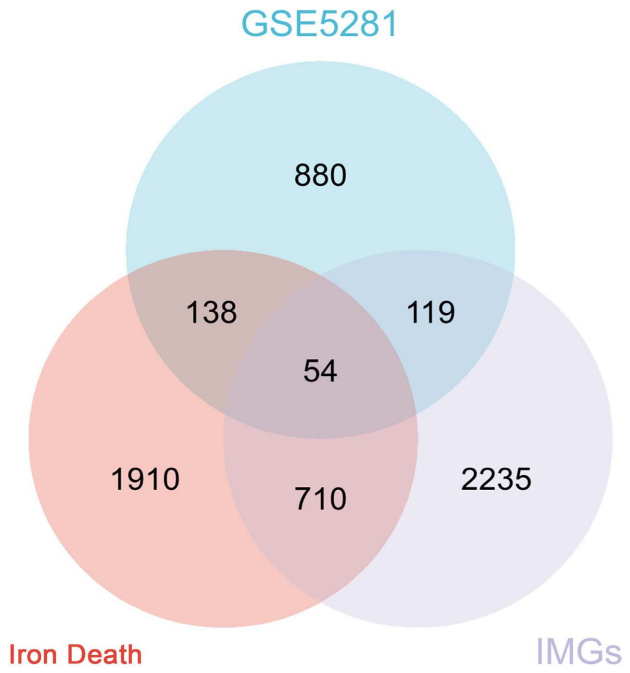

Figure 2. Identification of intersection genes between ferroptosis-related and immunity-related DEGs. Venn diagram of ferroptosis-immunity co-associated differentially expressed genes.

3.3. Validation of Expression Patterns of Candidate Genes

Bidirectional clustering was performed on the 54 IF-DEGs, and an expression heatmap was generated (Figure 3). The results showed that the expression patterns of these genes could clearly distinguish the AD group from the control group, with

convergent expression within groups and significant differences between groups. Some genes were upregulated in the AD group, while others were downregulated, consistent with the volcano plot results, indicating that this gene set has good discriminative ability between groups. The clustering heatmap did not detect obvious batch effects, suggesting that the preprocessing steps effectively removed systematic errors.

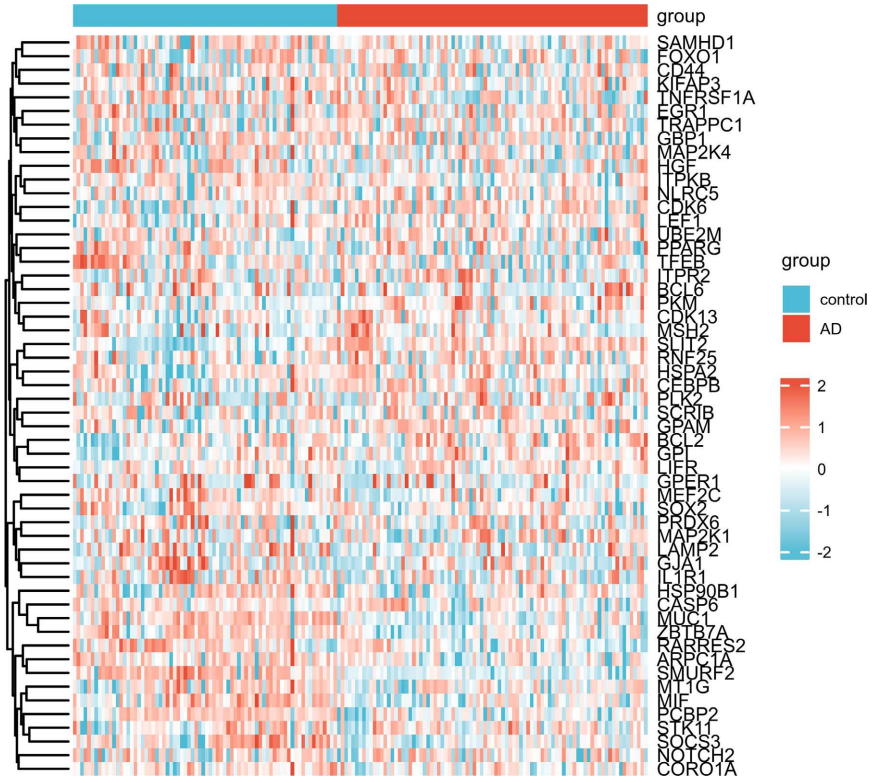

Figure 3. Validation of expression patterns of candidate genes. Expression pattern heatmap of candidate genes.

3.4. Functional Enrichment Analysis of Candidate Genes

To elucidate the biological functions of IF-DEGs, GO and KEGG enrichment analyses were conducted using clusterProfiler (adjusted $P < 0.05$).

The results for the three GO subcategories are as follows: In the biological process (BP) category, genes were enriched in terms such as negative regulation of immune system process, monocyte differentiation, and lymphocyte proliferation, suggesting that candidate genes are involved in immune-inflammatory regulation in AD (**Figure 4(a)**); In the cellular component (CC) category, enrichment was found in vesicle lumen and secretory granule lumen, indicating their functions are related to vesicle transport and secretion processes (**Figure 4(b)**); In the molecular function (MF) category, genes were concentrated in DNA-binding transcription factor binding, RNA polymerase II-specific transcription factor binding, and transcription co-regulator binding, suggesting that candidate genes primarily play transcriptional regulatory roles (**Figure 4(c)**).

KEGG pathway enrichment showed: the outer ring represents significantly enriched KEGG pathway IDs, the inner ring color indicates the overall regulatory direction of the pathway (Z-score, red for upregulation, purple for downregulation); outer ring scatter points represent enriched genes within the pathway, with purple dots for upregulated genes and red dots for downregulated genes. Results indicated that IF-DEGs were mainly enriched in the TNF signaling pathway, lipid metabolism-related pathways, and immune-inflammatory pathways, suggesting that candidate genes participate in the pathological process of AD by regulating these pathways (**Figure 4(d)**).

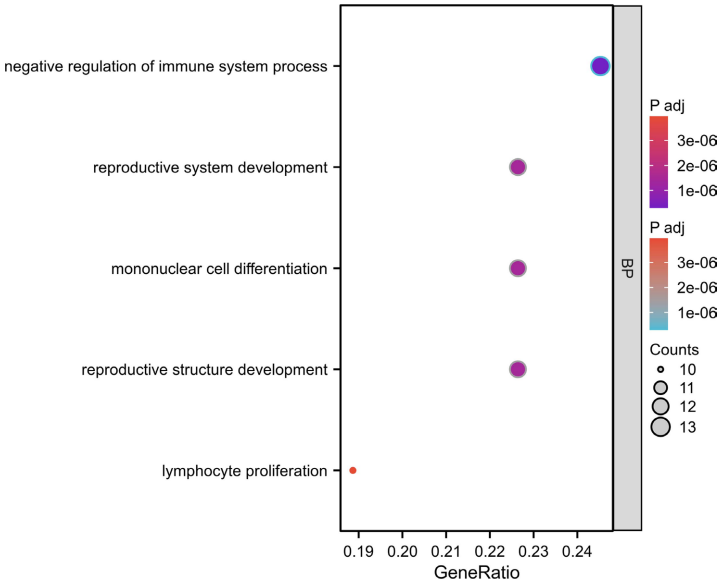

(a)

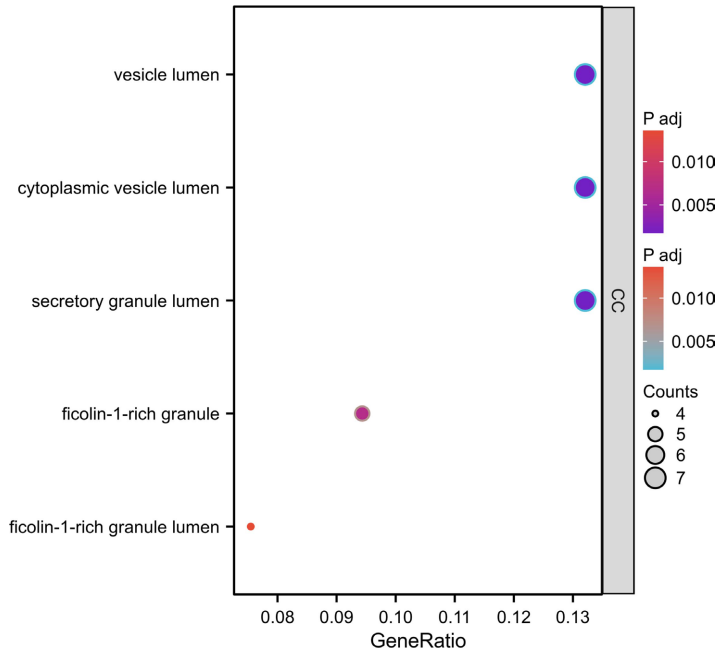

(b)

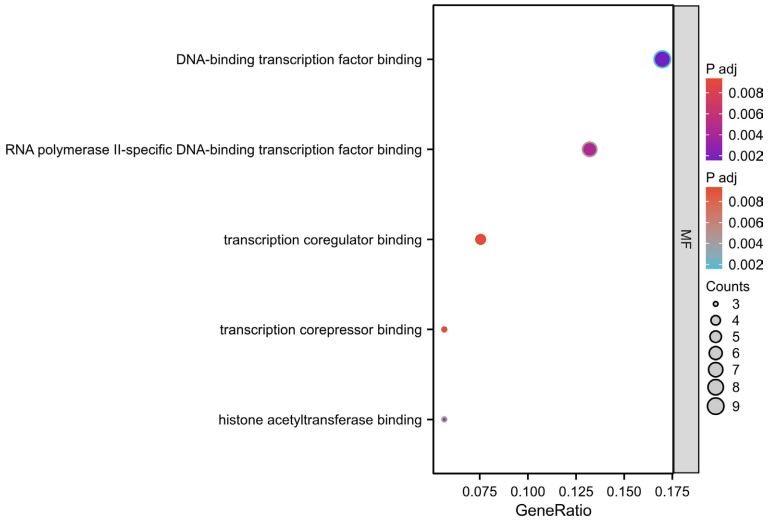

(c)

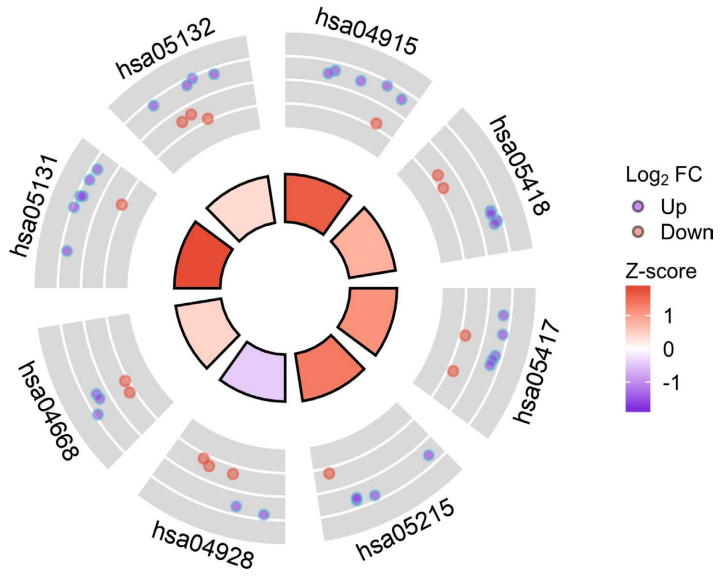

(d)

Figure 4. Functional enrichment analysis of candidate genes. (a) GO enrichment biological process diagram of candidate genes; (b) GO enrichment cellular component diagram of candidate genes; (c) GO enrichment molecular function diagram of candidate genes; (d) KEGG enrichment circle diagram of candidate genes.

3.5. PPI Network Construction and Core Gene Identification

The 54 IF-DEGs were submitted to the STRING database to construct a PPI network with a confidence score ≥ 0.7, containing 54 nodes and 217 interaction edges, with no isolated nodes (**Figure 5**). Using Cytoscape and the CytoHubba plugin, combined with the MCC algorithm and node connectivity, the top 5 core Hub genes were screened: BCL2, CD44, FOXO1, PPARG, and SOX2. These genes had the highest connectivity in the network and extensive interactions with other candidate genes, suggesting their pivotal role in the ferroptosis-immunity cross-regulation in AD.

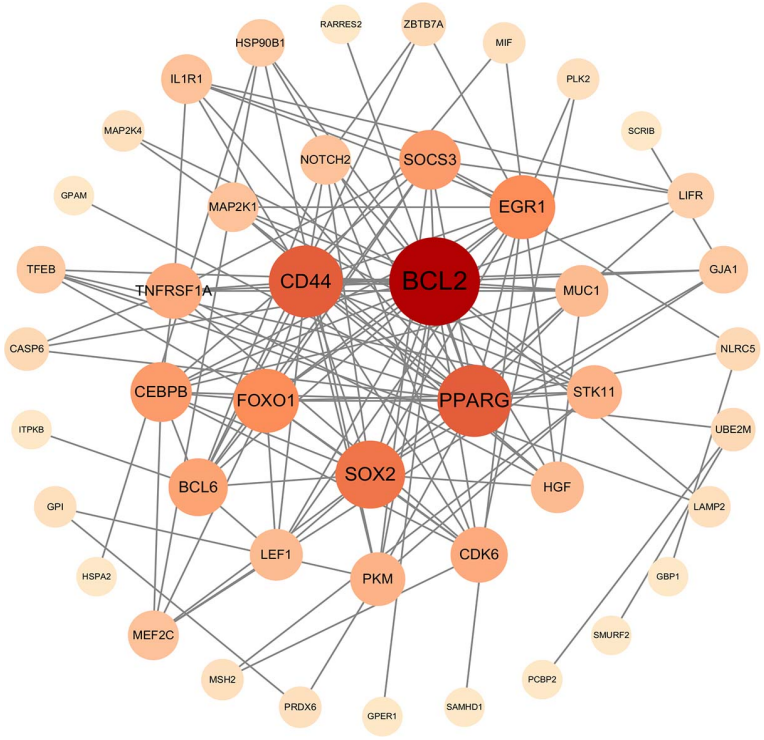

Figure 5. PPI network construction and core gene identification. PPI network and core genes of candidate genes.

3.6. Genome-Wide Pathway Enrichment Analysis

To compensate for the limitation of traditional differential gene enrichment analysis, which only focuses on screened genes, GSEA was performed based on the whole gene expression profile using KEGG and Reactome gene sets, with adjusted $P < 0.05$ as the threshold to identify significantly activated or inhibited pathways in the AD group.

Among significantly inhibited pathways, DNA replication, DNA synthesis, G2/M cell cycle checkpoint, removal of ORC1 from chromatin, SCF-SKP2-mediated degradation of P27/P21, Dectin-1-mediated non-canonical NF-κB signaling, and host interaction of HIV factors from the Reactome database were all negatively enriched. Pathway interaction networks showed close functional associations among these pathways, collectively involved in cell cycle regulation, DNA replication, and innate immune signaling (**Figure 6(a)**). The NES bar chart further quantified the inhibition degree of each pathway (NES range −2.431 to −2.39) (**Figure 6(d)**). Among them, the inhibition of neurotransmitter receptors and postsynaptic signal transduction pathways was the most significant (NES = −2.523), with a continuously declining enrichment curve, consistent with the pathological features of impaired synaptic function and neurotransmitter transmission disorders in AD (**Figure 6(b)**, **Figure 6(c)**).

Among significantly activated pathways, the cytokine-cytokine receptor interaction pathway (NES = 2.484) and the SUMOylation pathway (NES = 2.404) had the highest enrichment. The enrichment curve of the former continuously rose,

indicating overall activation of this pathway in the AD group, corroborating the increased proportion of pro-inflammatory immune cells in immune infiltration analysis; the latter is involved in protein post-translational modification and homeostasis regulation, and its abnormal activation may be related to the accumulation of misfolded proteins in AD (**Figure 6(b)**, **Figure 6(c)**).

The ridge plot and bar chart, respectively, displayed the distribution characteristics of NES values and enrichment degrees of each pathway, with consistent results, collectively revealing the overall transcriptomic features of AD, including activation of immune-inflammatory pathways and inhibition of synaptic and cell cycle-related pathways (**Figure 6(c)**, **Figure 6(d)**).

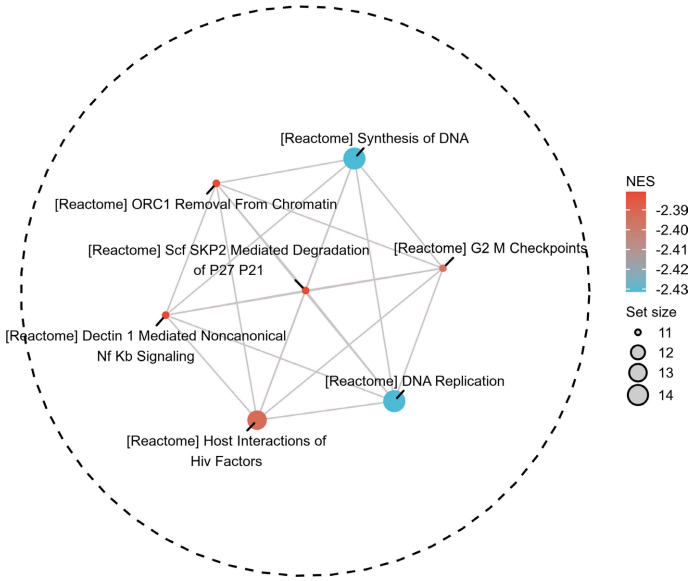

(a)

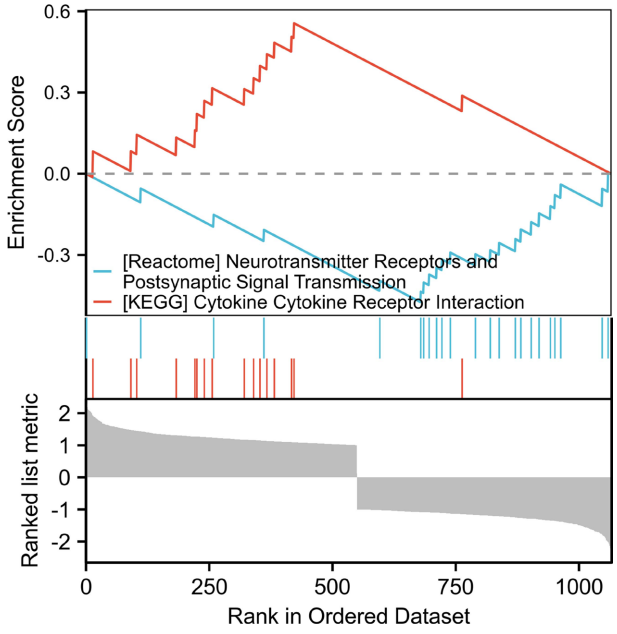

(b)

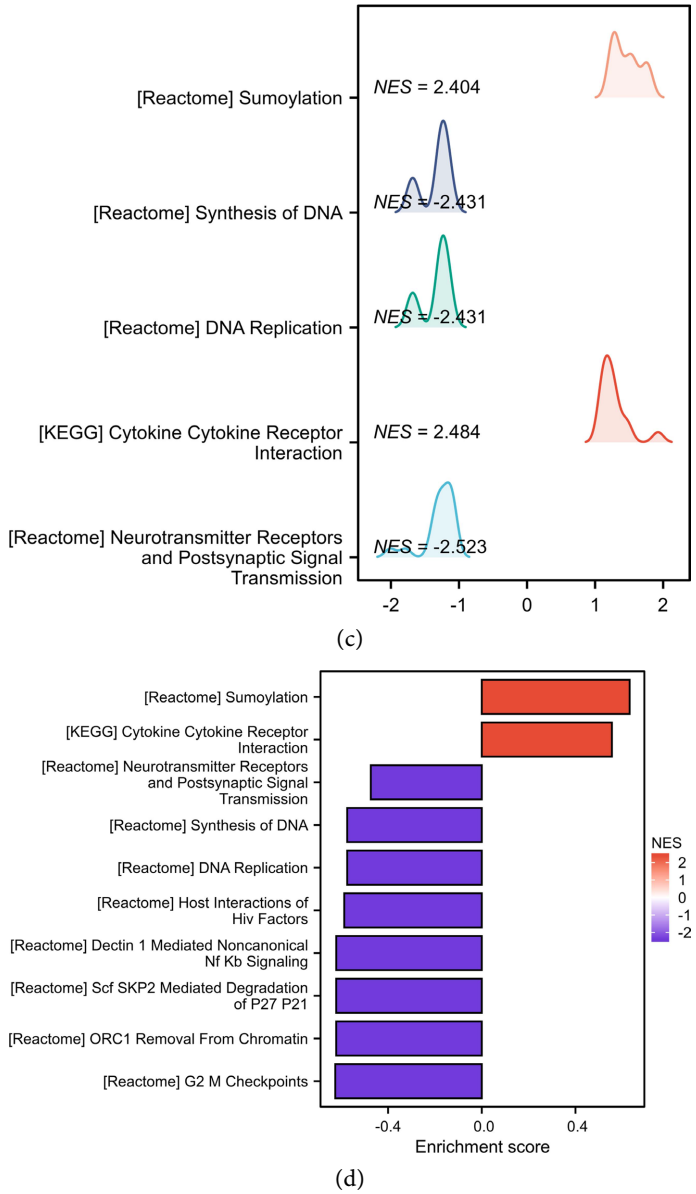

Figure 6. Genome-wide pathway enrichment analysis. (a) Interaction network diagram of significantly inhibited pathways; (b) GSEA enrichment curves of key pathways; (c) Ridge plot of NES distribution for significant pathways; (d) Bar chart of NES for significant pathways.

3.7. Analysis of Immune Cell Infiltration Characteristics

The CIBERSORT algorithm was used to estimate the relative infiltration abundance of 22 immune cell types in the AD group and the control group. Stacked bar charts showed significant differences in immune cell composition between the two groups, with an overall increase in the proportion of pro-inflammatory activated immune cells in the AD group (**Figure 7(a)**). Box plots further indicated that compared to the control group, the proportions of memory B cells, $CD8^+$ cytotoxic T cells, eosinophils, and neutrophils were significantly increased in the AD group (FDR-adjusted $P < 0.05$, $P < 0.001$); while the proportions of follicular helper

T cells, resting NK cells, and M0/M1/M2 macrophages were significantly decreased (FDR-adjusted P < 0.05, *P < 0.01, **P < 0.001) (Figure 7(b)). These results suggest remodeling of the immune microenvironment in AD brain tissue, with increased infiltration of pro-inflammatory immune cells coexisting with a decrease in homeostatic immune cells, constituting the cellular basis of central immune imbalance.

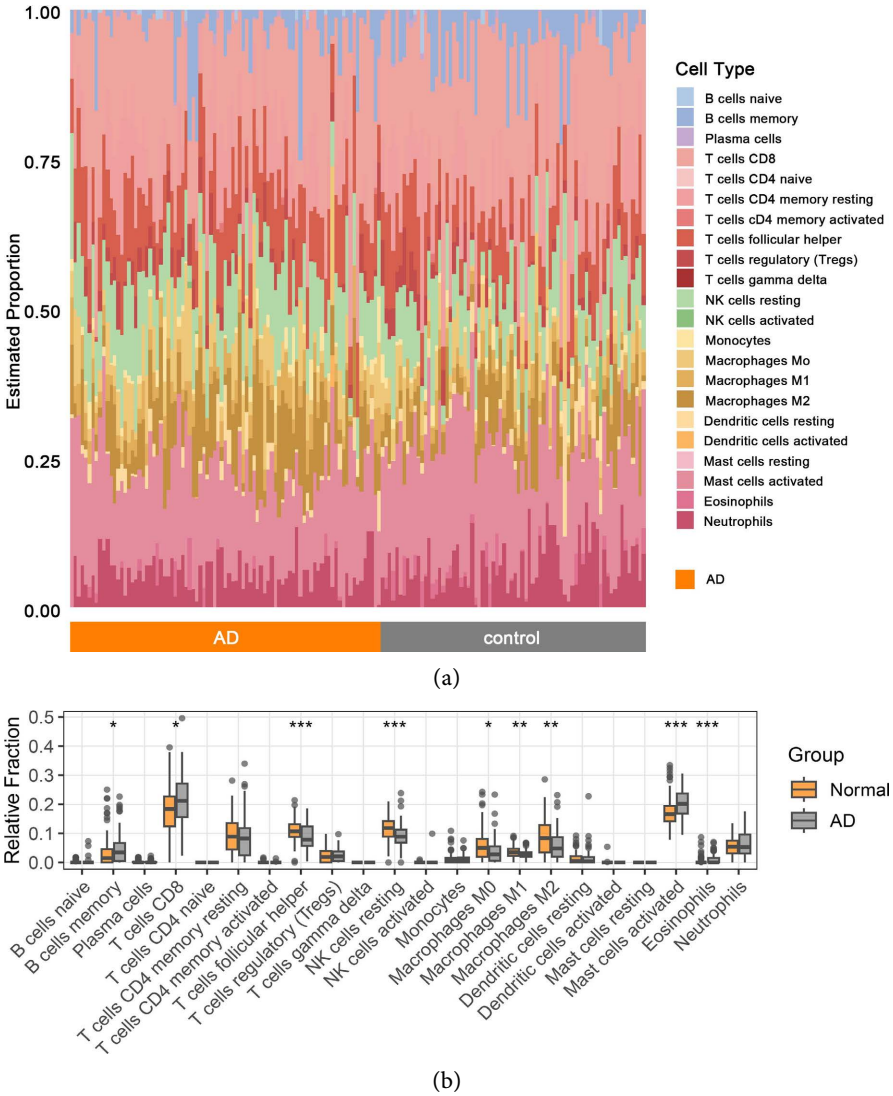

Figure 7. Analysis of immune cell infiltration characteristics. (a) Stacked bar chart of immune cell infiltration composition in AD and control group samples; (b) Box plot of intergroup differences in immune cell infiltration levels between AD and control groups.

4. Discussion

The pathogenesis of AD involves multiple pathological processes, including β-amyloid deposition, hyperphosphorylation of the Tau protein, iron metabolism disorders, and neuroinflammation. Ferroptosis, an iron-dependent form of programmed cell death, plays a key role in the onset of AD [8] [9]; immune microen-

vironment disturbances are also considered important pathological markers of AD [10]. However, the synergistic regulatory mechanisms between ferroptosis and immune responses in AD remain unclear. Based on the GSE5281 dataset, this study integrated multiple bioinformatics methods to identify 54 ferroptosis-immune co-expressed differentially expressed genes and focused on five core Hub genes—BCL2, CD44, FOXO1, PPARG, and SOX2—providing new molecular evidence for understanding the cross-talk mechanisms between ferroptosis and immune regulation in AD.

Functional enrichment analysis revealed that the candidate genes were significantly enriched in the TNF signaling pathway, lipid metabolism-related pathways, and immune-inflammatory pathways. The TNF pathway is a classic hub connecting inflammation and cell death; its activation can induce mitochondrial dysfunction and reactive oxygen species (ROS) accumulation through downstream signaling cascades, and excessive ROS production is one of the core triggers of ferroptosis [11] [12]. The enrichment of lipid metabolism pathways aligns closely with the essential characteristics of ferroptosis: the execution phase of ferroptosis relies on membrane phospholipid peroxidation, and lipid metabolism disorders can directly provide the substrate basis. Presenilin mutations can selectively sensitize cells to ferroptosis by inhibiting GPX4 expression, further supporting the critical role of these pathways in AD [3]. Additionally, the enrichment of the "vesicle lumen" component suggests that candidate genes may be involved in exosome-mediated intercellular communication. Studies have shown that damage-associated molecular patterns released during ferroptosis can be transmitted between neurons and glial cells via exosomes, driving microglial activation and T-cell infiltration, leading to systemic immune imbalance [2]. Overall, these results reveal an inflammation-ferroptosis positive feedback mechanism driven by TNF signaling, involving abnormal lipid metabolism and mediated by vesicular transport.

In the protein-protein interaction (PPI) network analysis, we used the CytoHubba plugin in Cytoscape, employing the MCC algorithm combined with connectivity ranking, to identify five core Hub genes—BCL2, CD44, FOXO1, PPARG, and SOX2—further narrowing down the key nodes in ferroptosis-immune interactive regulation. Beyond its anti-apoptotic function, BCL2 can negatively regulate autophagy by binding to Beclin-1, indirectly affecting ferritin degradation and intracellular iron pool levels [7]. CD44, as a hyaluronic acid receptor, not only participates in immune cell migration and homing but also regulates cellular iron uptake by interacting with transferrin receptors, forming a direct link between immunity and iron metabolism [4]. PPARG is a master regulator of lipid metabolism and inflammatory responses; Tang *et al.*, through integrated multi-omics analysis, explicitly proposed that PPARG is a key hub connecting ferroptosis and neuroinflammation [13]. In this study, PPARG expression was downregulated in the AD group and consistent with the decreasing trend of M2 macrophages, suggesting it may primarily play a protective role. Abnormal activation of the NLRP3 inflammasome has been confirmed to simultaneously participate in pyroptosis and

ferroptosis induction, providing another important interface for inflammation-ferroptosis interactive regulation [5]. FOXO1 and SOX2 are involved in T-cell function regulation and neural stem cell fate determination, respectively, and their abnormal expression may lead to immune cell functional imbalance [7].

Immune infiltration analysis provided cellular-level corroboration for the above molecular findings. This study found that the proportions of memory B cells, $CD8^+$ T cells, eosinophils, and neutrophils were significantly increased in AD brain tissues, while the proportions of follicular helper T cells, resting NK cells, and M0/M1/M2 macrophages were significantly decreased. These results are partially consistent with previous studies on immune infiltration in AD [14] [15]. The pattern of increased pro-inflammatory and cytotoxic immune cells and decreased homeostatic immune cells suggests that the brain in AD is not simply in a state of "inflammation activation" but rather a more complex "immune imbalance". Yang *et al.* confirmed in the SAMP8 mouse model that activating the Nrf2/GPX4 axis could simultaneously inhibit ferroptosis and reduce $CD8^+$ T-cell infiltration, indicating functional coupling between ferroptosis and adaptive immunity [6]. He *et al.*'s integrated single-cell and bulk RNA analysis also revealed changes in immune cell expression patterns in the AD immune microenvironment [16]. On the other hand, the decreasing trends of all three macrophage subsets in the AD group suggest a potential widespread decline in overall macrophage function. Sing *et al.* found that the TRPM8 channel in microglia could affect ferroptosis and M1-M2 polarization by regulating transferrin-mediated iron uptake, providing a new perspective for understanding iron metabolism regulation in immune cells themselves [4].

This study has several limitations. First, the GSE5281 dataset pools samples from multiple brain regions, including the hippocampus and temporal cortex. In our limma differential analysis design, we included only disease status as a grouping variable and did not statistically correct for brain region heterogeneity; this potential confounder may bias the identification of differentially expressed genes, and future studies should employ more rigorous comparison models or brain region matching strategies. The data source is limited to the single microarray dataset GSE5281, lacking independent external validation; the robustness of the conclusions needs to be tested in more datasets. Tissue homogenate microarray data cannot distinguish the cellular origins of gene changes, limiting the cellular resolution of mechanistic analysis. Existing studies have begun to use single-cell sequencing technology to reveal differences in ferroptosis susceptibility among different cell types in AD [16]. Additionally, bioinformatics analysis reveals correlations at the transcriptome level rather than causal relationships; the functions of Hub genes still require validation through gene intervention experiments and AD animal models. Maimaiti *et al.* have confirmed the role of NOX4-mediated astrocyte ferroptosis in AD at the cellular level, providing methodological references for subsequent functional validation [17]; although therapeutic strategies targeting ferroptosis are promising, their translational application still faces multiple

challenges.

In summary, this study constructed a multi-level molecular network of ferroptosis-immune interactive regulation in AD, identified five core Hub genes—BCL2, CD44, FOXO1, PPARG, and SOX2—revealed an inflammation-ferroptosis positive feedback mechanism driven by the TNF signaling pathway and abnormal lipid metabolism, and described the remodeling pattern of the immune microenvironment in AD brain tissues characterized by increased pro-inflammatory immune cell infiltration and a comprehensive reduction in macrophages. These findings provide a theoretical basis and candidate targets for the development of early diagnostic markers and combined immune-ferroptosis targeting strategies for AD.

5. Conclusion

This study found that BCL2, CD44, FOXO1, PPARG, and SOX2 are potential core Hub genes in ferroptosis-immune interactive regulation in AD. Their functions mainly involve the TNF signaling pathway, lipid metabolism-related pathways, and immune-inflammatory pathways, suggesting that these genes may participate in the pathological process of AD by synergistically regulating the inflammation-ferroptosis positive feedback loop. The immune microenvironment remodeling characteristics revealed by immune infiltration analysis—increased infiltration of pro-inflammatory immune cells and reduced macrophages in AD brain tissues—provide cellular-level evidence for understanding central immune imbalance in AD. These findings offer novel bioinformatics insights into the interaction between ferroptosis and immunity in AD pathogenesis, and the identified hub genes may serve as potential candidate targets for future functional validation and targeted research. Simultaneously, this study enriches research on the pathological mechanisms of the interaction between ferroptosis and the immune microenvironment in AD, providing a new theoretical basis and research direction for clinical targeted immune-iron metabolism combined intervention, which is of great significance for optimizing early diagnosis and precision treatment strategies for AD.

Conflicts of Interest

The authors declare no conflicts of interest regarding the publication of this paper.

References

[1] He, Y., Cong, L., Liang, S., Ma, X., Tian, J., Li, H., *et al.* (2022) Discovery and Validation of Ferroptosis-Related Molecular Patterns and Immune Characteristics in Alzheimer's Disease. *Frontiers in Aging Neuroscience*, **14**, Article ID: 1056312. https://doi.org/10.3389/fnagi.2022.1056312

[2] Zhou, Z., Zhang, Y., Liu, S., Tang, H., Yang, L., Lu, Y., *et al.* (2025) Ferroptosis in Alzheimer's Disease: Molecular Mechanisms and Advances in Therapeutic Strategies. *Frontiers in Neuroscience*, **19**, Article ID: 1673315. https://doi.org/10.3389/fnins.2025.1673315

[3] Greenough, M.A., Lane, D.J.R., Balez, R., Anastacio, H.T.D., Zeng, Z., Ganio, K., *et al.* (2022) Selective Ferroptosis Vulnerability Due to Familial Alzheimer's Disease Presenilin Mutations. *Cell Death & Differentiation*, **29**, 2123-2136. https://doi.org/10.1038/s41418-022-01003-1

[4] Sing, R., Shikha, D. and Goswami, C. (2025) TRPM8 Modulation Alters Uptake of Transferrin-Mediated Fe^{3+}, Mitochondrial Fe^{2+} and Intracellular Ca^{2+}-Levels in Microglia. *Neurochemistry International*, **189**, Article 106031. https://doi.org/10.1016/j.neuint.2025.106031

[5] Huang, Y., Xu, W. and Zhou, R. (2021) NLRP3 Inflammasome Activation and Cell Death. *Cellular & Molecular Immunology*, **18**, 2114-2127. https://doi.org/10.1038/s41423-021-00740-6

[6] Yang, S., Wang, L., Zeng, Y., Wang, Y., Pei, T., Xie, Z., *et al.* (2023) Salidroside Alleviates Cognitive Impairment by Inhibiting Ferroptosis via Activation of the NRF2/GPX4 Axis in SAMP8 Mice. *Phytomedicine*, **114**, Article 154762. https://doi.org/10.1016/j.phymed.2023.154762

[7] Sun, Y., Xiao, Y., Tang, Q., *et al.* (2024) Genetic Markers Associated with Ferroptosis in Alzheimer's Disease. *Frontiers in Aging Neuroscience*, **16**, Article ID: 1364605. https://doi.org/10.3389/fnagi.2024.1364605

[8] Feng, L., Sun, J., Xia, L., Shi, Q., Hou, Y., Zhang, L., *et al.* (2024) Ferroptosis Mechanism and Alzheimer's Disease. *Neural Regeneration Research*, **19**, 1741-1750. https://doi.org/10.4103/1673-5374.389362

[9] Zhang, G., Zhang, Y., Shen, Y., Wang, Y., Zhao, M. and Sun, L. (2021) The Potential Role of Ferroptosis in Alzheimer's Disease. *Journal of Alzheimer's Disease*, **80**, 907-925. https://doi.org/10.3233/jad-201369

[10] Chen, H., Zhao, Y. and Xie, Y. (2023) Immunosenescence of Brain Accelerates Alzheimer's Disease Progression. *Reviews in the Neurosciences*, **34**, 85-101. https://doi.org/10.1515/revneuro-2022-0021

[11] Maheshwari, S. (2023) Ferroptosis Signaling Pathways: Alzheimer's Disease. *Hormone and Metabolic Research*, **55**, 819-826. https://doi.org/10.1055/a-2084-3561

[12] Chen, K., Jiang, X., Wu, M., Cao, X., Bao, W. and Zhu, L. (2021) Ferroptosis, a Potential Therapeutic Target in Alzheimer's Disease. *Frontiers in Cell and Developmental Biology*, **9**, Article ID: 704298. https://doi.org/10.3389/fcell.2021.704298

[13] Tang, L., Wu, N., Xu, H. and Mo, Y. (2026) PPARG as a Central Regulator of Ferroptosis in Alzheimer's Disease: Integrated Transcriptomic, Single-Cell, and Experimental Evidence. *Frontiers in Aging Neuroscience*, **18**, Article ID: 1759279. https://doi.org/10.3389/fnagi.2026.1759279

[14] Zhang, H., Cao, S., Xu, Y., Sun, X., Fei, M., Jing, Q., *et al.* (2022) Landscape of Immune Infiltration in Entorhinal Cortex of Patients with Alzheimer's Disease. *Frontiers in Pharmacology*, **13**, Article ID: 941656. https://doi.org/10.3389/fphar.2022.941656

[15] Liu, P., Huang, C., Lu, L., Pang, Y.L. and Huang, Z. (2026) Integrated Transcriptomic Analysis of the Temporal Cortex Identifies CRH and GAD2 as Neuropathological Markers and Reveals Altered Immune Microenvironment in Alzheimer's Disease. *Scientific Reports*, **16**, Article No. 10438. https://doi.org/10.1038/s41598-026-40762-6

[16] He, H., Yang, Y., Wang, L., Guo, Z., Ye, L., Ou-Yang, W., *et al.* (2023) Combined Analysis of Single-Cell and Bulk RNA Sequencing Reveals the Expression Patterns of Circadian Rhythm Disruption in the Immune Microenvironment of Alzheimer's Disease. *Frontiers in Immunology*, **14**, Article ID: 1182307.

https://doi.org/10.3389/fimmu.2023.1182307

[17] Maimaiti, Y., Su, T., Zhang, Z., Ma, L., Zhang, Y. and Xu, H. (2024) Nox4-Mediated Astrocyte Ferroptosis in Alzheimer's Disease. *Cell & Bioscience*, **14**, Article No. 88. https://doi.org/10.1186/s13578-024-01266-w